

Photonuclear reactions of three-nucleon systems

W. Schadow,¹ O. Nohadani,² and W. Sandhas²

¹TRIUMF, 4004 Wesbrook Mall, Vancouver, British Columbia, Canada V6T 2A3

²Physikalisches Institut der Universität Bonn, Endenicher Allee 11-13, D-53115 Bonn, Germany

(Received 28 June 2000; published 14 March 2001)

We discuss the available data for the differential and the total cross section for the photodisintegration of ${}^3\text{He}$ and ${}^3\text{H}$ and the corresponding inverse reactions below $E_\gamma = 100$ MeV by comparing with our calculations using realistic NN interactions. The theoretical results agree within the error bars with the data for the total cross sections. Excellent agreement is achieved for the angular distribution in the case of ${}^3\text{He}$, whereas for ${}^3\text{H}$ a discrepancy between theory and experiment is found.

DOI: 10.1103/PhysRevC.63.044006

PACS number(s): 21.45.+v, 25.40.Lw, 25.20.-x, 27.10.+h

I. INTRODUCTION

Over the last decades the photodisintegration of ${}^3\text{He}$ and ${}^3\text{H}$ and the corresponding inverse reactions have been investigated experimentally and theoretically with considerable interest. There have been a lot of experiments using different techniques for the photodisintegration of ${}^3\text{He}$ [1–21] and ${}^3\text{H}$ [22–28] or the inverse reaction, respectively. Despite the many investigations, there are inconsistencies between the data up to 30% in the magnitudes of the cross sections.

Early theoretical calculations were restricted to phenomenological interactions and various approximations in the bound state wave function and the scattering states (for a list of references see Ref. [29]). The first consistent calculation for both the initial and the final state was done by Gibson and Lehman [30]. They solved Faddeev-type Alt-Grassberger-Sandhas (AGS) equations [31] using Yamaguchi interactions and taking into account only the $E1$ contributions of the electromagnetic interaction.

Attempts to use realistic interactions are the ones by Aulfleger and Drechsel [32] and by Craver *et al.* [33]. In both calculations higher multipoles were considered, but the three-body scattering state was not treated exactly. The unusual energy dependence of the cross section postulated by Craver *et al.* has never been confirmed by any other calculation. Klepacki *et al.* [29] also used a realistic interaction, however, in plane wave impulse approximation. King *et al.* [13] performed an effective two-body direct capture calculation with the initial state being treated as a plane wave, or as a scattering state generated from an optical potential.

The very-low-energy n - d radiative capture process is dominated by the magnetic dipole ($M1$) transition, and has been studied by several authors [34,35] in configuration-space with inclusion of three-body forces, final state interaction (FSI), and explicit meson exchange currents (MEC). The inclusive reaction (two- and three-fragment) has been studied recently by Efros *et al.* [36] with realistic two-body interactions and three-body forces as input in the energy range up to 100 MeV by employing the Lorentz integral transformation method. Other recent theoretical work was devoted to polarization observables for p - d capture [37–41] using realistic interactions. A discussion of polarization observables will be published in a subsequent paper.

In Refs. [42–44], we have treated the ${}^3\text{He}$ and ${}^3\text{H}$ pho-

todisintegration and the inverse processes, i.e., the radiative capture of protons or neutrons by deuterons, within the integral equation approach discussed below. These calculations were based on the Bonn A , Bonn B , and Paris potentials in Ernst-Shakin-Thaler (EST) expansion: Bonn A (EST), Bonn B (EST), and Paris (EST) [45,46]. We have demonstrated, in particular, the role of $E2$ contributions, meson exchange currents, and higher partial waves. A noticeable potential dependence was found in the peak region, i.e., for $E_x \leq 20$ MeV. But it was also shown that the different peak heights are strongly correlated with the different three-nucleon binding energies obtained for the potentials employed. The possibility of using the magnitudes of the cross sections as an independent test of the quality of the potentials, thus, appears rather restricted.

The aim of the present paper is to extend the investigations of Refs. [42–44] to photon energies from 20 to 100 MeV. Aside from certain energy points there are up to now no other theoretical calculations for the differential and the total cross section available in this energy range using the full final-state amplitudes, realistic interactions, and taking into account $E1$ and $E2$ contributions of the electromagnetic interaction.

This paper is organized as follows. In Sec. II we present the theoretical framework of our calculations. The results are discussed in Sec. III. Our conclusions are summarized in Sec. IV.

II. THEORY

The amplitude for the two-fragment photodisintegration of ${}^3\text{H}$ or ${}^3\text{He}$ into a deuteron ψ_d and a neutron or proton of relative momentum \mathbf{q} is given by

$$M(\mathbf{q}) = {}_S^{(-)}\langle \mathbf{q}; \psi_d | H_{\text{em}} | \Psi_{\text{BS}} \rangle_S = {}_S^{(-)}\langle \Psi | H_{\text{em}} | \Psi_{\text{BS}} \rangle_S. \quad (1)$$

Here $|\Psi_{\text{BS}}\rangle_S$ represents the incoming three-nucleon bound state while ${}_S^{(-)}\langle \mathbf{q}; \psi_d |$ denotes the final continuum (scattering) state with outgoing boundary condition. H_{em} is the electromagnetic operator. The antisymmetrized final state can be represented as a sum over the three possible two-fragment partitions β

$${}^{(-)}\langle \mathbf{q}; \psi_d | = {}^{(-)}\langle \Psi | = \frac{1}{\sqrt{3}} \sum_{\beta} {}^{(-)}\langle \Psi_{\beta} |. \quad (2)$$

The scattering state ${}^{(-)}\langle \Psi_{\beta} |$ can be obtained from the free channel state $\langle \Phi_{\beta} | = \langle (\beta) \mathbf{q} | \langle (\beta) \psi_d |$ via the Møller operators $\Omega_{\beta}^{(-)}$, i.e., ${}^{(-)}\langle \Psi_{\beta} | = \langle \Phi_{\beta} | \Omega_{\beta}^{(-)\dagger}$. It can be shown [47] that the adjoint Møller operators satisfy the relation

$$\Omega_{\beta}^{(-)\dagger} = \delta_{\beta\alpha} + U_{\beta\alpha}(E_{\beta} + i0)G_{\alpha}(E_{\beta} + i0), \quad (3)$$

where $U_{\beta\alpha}$ are the usual AGS [31] operators, and G_{α} is the resolvent of the channel Hamiltonian $H_{\alpha} = H_0 + V_{\alpha}$. In this notation $V_{\alpha} = V_{\beta\gamma}$ denotes the interaction between the particle β and γ , while H_0 denotes the free three-body Hamiltonian. In order to find a set integral equations for the adjoint Møller operators we multiply the AGS equations

$$U_{\beta\alpha} = (1 - \delta_{\beta\alpha})G_0^{-1} + \sum_{\gamma} (1 - \delta_{\beta\alpha})T_{\gamma}G_0U_{\gamma\alpha} \quad (4)$$

from the right with G_{α} and add $\delta_{\beta\alpha}$ on both sides. Reordering terms, using the relation $T_{\gamma}G_0 = V_{\gamma}G_{\gamma}$ and Eq. (3) we end up with

$$\Omega_{\beta}^{(-)\dagger} = 1 + \sum_{\gamma} (1 - \delta_{\beta\gamma})T_{\gamma}G_0\Omega_{\gamma}^{(-)\dagger}. \quad (5)$$

These equations, sandwiched between an outgoing channel state $\langle \Phi_{\beta} |$ and the state $H_{\text{em}}|\Psi_{\text{BS}}\rangle$, go over into a set of effective two-body equations when representing the input two-body T operator in separable form. In order to accomplish this, we use the separable expansion method proposed by Ernst, Shakin, and Thaler [48] for representing a given NN interaction. In this scheme the original potential is expressed as a sum over separable terms

$$V_{ll'}^{\eta} = \sum_{\mu, \nu=1}^N |g_{\nu}^{\eta}l\rangle \Lambda_{\mu\nu}^{\eta} \langle g_{\nu}^{\eta}l' |, \quad (6)$$

where N is the rank of the separable representation, $\Lambda_{\mu\nu}$ are the coupling strengths, and $|g_{\nu}^{\eta}l\rangle$ are the form factors. Here l and l' are the orbital angular momenta. The total angular momentum j is obtained from the coupling sequence $(ls)j$, with s being the spin. The collective index η stands for the quantum numbers $(sj;t)$, where t is the isospin. Using this representation for the potential, the two-body T operator reads

$$T_{ll'}^{\eta}(E+i0) = \sum_{\mu\nu} |g_{\mu}^{\eta}l\rangle \Delta_{\mu\nu}^{\eta}(E+i0) \langle g_{\nu}^{\eta}l' |, \quad (7)$$

with

$$\Delta^{\eta}(E+i0) = [(\Lambda^{\eta})^{-1} - \mathcal{G}_0(E+i0)]^{-1} \quad (8)$$

and

$$[\mathcal{G}_0(E+i0)]_{\mu\nu} = \sum_l \langle g_{\mu}l | G_0(E+i0) | g_{\nu}l \rangle. \quad (9)$$

TABLE I. Ranks of the two-body partial waves of the Paris, Bonn A, and Bonn B potentials in EST representation used for the bound-state and the scattering calculations.

Partial wave	Bonn A (EST)	Bonn B (EST)	Paris (EST)
1S_0	5	5	5
${}^3S_1 - {}^3D_1$	6	6	6
1D_2	4	4	5
3D_2	4	4	5
1P_1	4	4	5
3P_1	4	4	5
3P_0	4	4	5
${}^3P_2 - {}^3F_2$	5	5	7

For more details of this construction we refer to Refs. [45,46]. The ranks for each partial wave used in this paper for the bound-state and the scattering calculations are contained in Table I. With proper normalized form factors the deuteron wave function is given by

$$|\psi_d\rangle = \sum_l G_0(E_d) |g_1^{\eta}l\rangle. \quad (10)$$

Equation (5) will be treated numerically in momentum space, employing a complete set of partial wave states $|pqlb\Gamma M_{\Gamma}; IM_I\rangle$. The label b denotes the set (ηSKL) of quantum numbers, where K and L are the channel spin of the three nucleons [with the coupling sequence $(jS)K$] and the relative angular momentum between the two-body subsystem and the third particle, respectively. The index S is the spin of the third particle. Γ is the total angular momentum following from the coupling sequence $(KL)\Gamma$, the total isospin I follows from the coupling $(t\tau)I$, where τ is the isospin of the third particle. The required antisymmetry under permutation of two particles in the subsystem can be achieved by choosing only those states which satisfy the condition $(-)^{l+s+t} = -1$.

Using the above defined states, the partial-wave decomposition of the channel state $\langle \Phi_{\beta} | = \langle (\beta) \mathbf{q} | SM_S; \tau M_{\tau} | \langle (\beta) \Psi^{\eta} m_j; m_l |$ reads

$$\begin{aligned} \langle \Phi_{\beta} | &= \sum_{\Gamma M_{\Gamma}} \sum_b \sum_{M_K M_L} \sum_{IM_I} Y_{LM_L}(\hat{q}) \langle jm_j SM_S | KM_K \rangle \\ &\times \langle KM_K LM_L | \Gamma M_{\Gamma} \rangle \langle tm_t \tau m_{\tau} | IM_I \rangle \\ &\times \langle (\beta) g_1 qb \Gamma M_{\Gamma}; IM_I | G_0(E_d + \frac{3}{4}q^2 + i0), \quad (11) \end{aligned}$$

with

$$\begin{aligned} &\langle (\beta) g_1 qb \Gamma M_{\Gamma}; IM_I | \\ &= \sum_l \int_0^{\infty} dp p^2 \langle (\beta) pqlb \Gamma M_{\Gamma}; IM_I | g_{1l}^{\eta}(p), \quad (12) \end{aligned}$$

where we have used Eq. (10) for the representation of the deuteron wave function. These states can be generalized to

arbitrary rank by replacing $\langle g_1 |$ with $\langle g_\mu |$. As the quantization axis we have chosen the direction of the incoming photon.

To derive an integral equation for the photodisintegration amplitudes we multiply Eq. (5) from the left with G_0 and the generalized states of Eq. (12), and from the right with $H_{\text{em}}|\Psi_{\text{BS}}\rangle_S$. After summing over the cluster index β we obtain

$$\begin{aligned} & \Gamma^I \mathcal{A} M_\mu^b(q, E_d + \frac{3}{4}q^2) \\ &= \Gamma^I \mathcal{A} B_\mu^b(q, E_d + \frac{3}{4}q^2) \\ &+ \sum_{b'} \sum_{\nu\rho} \int_0^\infty dq' q'^2 \Gamma^I \mathcal{A} V_{\mu\nu}^{bb'}(q, q', E_d + \frac{3}{4}q^2) \\ &\times \Delta_{\nu\rho}^{\eta'}(E_d + \frac{3}{4}q^2 - \frac{3}{4}q'^2) \Gamma^I \mathcal{A} M_\rho^{b'}(q', E_d + \frac{3}{4}q^2) \end{aligned} \quad (13)$$

with

$$\begin{aligned} \Gamma^I \mathcal{A} M_\mu^b(q, E) &= \frac{1}{\sqrt{3}} \sum_\beta \langle (\beta) g_\mu q b \Gamma; I | G_0(E + i0) \\ &\times \Omega_\beta^{(-)\dagger} H_{\text{em}} |\Psi_{\text{BS}}\rangle_S \end{aligned} \quad (14)$$

and

$$\begin{aligned} \Gamma^I \mathcal{A} B_\mu^b(q, E) &= \frac{1}{\sqrt{3}} \sum_\beta \langle (\beta) g_\mu q g b \Gamma; I | G_0(E + i0) \\ &\times H_{\text{em}} |\Psi_{\text{BS}}\rangle_S, \end{aligned} \quad (15)$$

where we have used the separable expansion of Eq. (7) for the T operator. Here $\Gamma^I \mathcal{A} B_\mu^b$ represents the so-called plane-wave (Born) amplitude and $\Gamma^I \mathcal{A} M_\mu^b$ denotes the full final-state amplitude. The effective potential $\Gamma^I \mathcal{A} V_{\mu\nu}^{bb'}$ entering Eq. (13) is given by

$$\begin{aligned} \Gamma^I \mathcal{A} V_{\mu\nu}^{bb'}(q, E) &= \sum_\beta (1 - \delta_{\beta\gamma}) \langle (\beta) g_\mu q b \Gamma; I | G_0(E + i0) | \\ &\times g_\nu q' b' \Gamma'; I'(\gamma) \rangle. \end{aligned} \quad (16)$$

The recoupling coefficients entering this equation can be found in Refs. [49,50]. In Eqs. (13)–(16) we have used the fact that the Born term, the effective potential, and therefore the full amplitude are diagonal in the quantum numbers Γ , M_Γ , I , and M_I .

In order to be able to solve Eq. (13) numerically an off-shell extension is required. This can easily be achieved by replacing $E_d + \frac{3}{4}q^2$ with the energy parameter E . The solution of Eq. (13) is obtained on the real axis by expanding the solution in cubic B splines [51] and solving a system of linear equations for the unknown coefficients.

In the Born amplitude one finds that the terms in the summation are independent from the partition, i.e., the summation over the different clusters can be replaced by a factor of 3. Using the generalized states of Eq. (12) we obtain

TABLE II. Calculated binding energies for the three-nucleon bound state. The total angular momentum of the two-body subsystem was restricted to $j \leq 2$.

Bonn A (EST)	Bonn B (EST)	Paris (EST)
−8.284	−8.088	−7.3688

$$\begin{aligned} \Gamma^I \mathcal{A} B_\mu^b(q, E) &= \sqrt{3} \sum_I \int dp p^2 \frac{g_{I\mu}^\eta(p)}{E - p^2 - \frac{3}{4}q^2 + i0} \\ &\times \langle p q l b \Gamma; I | H_{\text{em}} |\Psi_{\text{BS}}\rangle_S. \end{aligned} \quad (17)$$

Our treatment of the three-nucleon bound state $|\Psi_{\text{BS}}\rangle$ which is contained in the expression for the Born amplitude is described in Refs. [52,53]. The obtained binding energies for the three potentials used in this paper can be found in Table II. As shown in [53] these values are practically the same as those for the original potentials. For the present calculation of the Faddeev components the total angular momentum j of the two-body potential was restricted to $j \leq 2$ (18 channels), while in the full state all partial waves with $j \leq 4$ (34 channels) have been taken into account. With this number of channels converged calculations of the observables for the photoprocesses in this paper were achieved, incorporating 99.8% of the wave functions [42,43]. For more details concerning the properties of the wave functions and their high quality we refer to Ref. [53].

The relevant electromagnetic operator in the total cross section at low energies is a dipole operator. In the differential cross section and at higher energies also the quadrupole operator is relevant. In order to take into account meson exchange currents we use Siegert's theorem [54], then these operators are given by [55]

$$H_{\text{em}}^{(1)} = -\mathcal{N} \sqrt{\frac{4\pi}{3}} i E_\gamma \sum_{i=1}^3 e_i r_i Y_{1\lambda}(\vartheta_i, \varphi_i) \quad (18)$$

and

$$H_{\text{em}}^{(2)} = \mathcal{N} \sqrt{\frac{4\pi}{3}} \frac{E_\gamma^2}{\sqrt{20}} \sum_{i=1}^3 e_i r_i^2 Y_{2\lambda}(\vartheta_i, \varphi_i), \quad (19)$$

where E_γ denotes the photon energy. Here, r_i are the nucleon coordinates, e_i the electric charges, and $\lambda = \pm 1$ is the polarization of the photon. The normalization factor \mathcal{N} contains the quantization volume and is canceled out in the calculation of the cross sections. For the calculation of matrix elements of these operators with initial and final state they need to be transformed into the three-body center-of-mass system. Expressions for the matrix elements can be found in Ref. [56].

The on-shell amplitudes can be obtained from

$$\begin{aligned}
 & \langle_S^{(-)} \langle \mathbf{q} S M_S; \psi_d j m_j | H_{\text{em}} | \Psi_{\text{BS}} \Gamma' M_{\Gamma'} \rangle_S \rangle \\
 &= \sum_{\Gamma=1/2}^{5/2} \sum_{M_{\Gamma}} \sum_b \sum_{M_K M_L} Y_{L M_L}(\hat{q}) \langle j m_j S M_S | K M_K \rangle \\
 & \quad \times \langle K M_K L M_L | \Gamma M_{\Gamma} \rangle^{\Gamma} A M_1^b(q, E_d + \frac{3}{4} q^2). \quad (20)
 \end{aligned}$$

In the summation of course only those channels contribute that have a deuteron as their subsystem. With these amplitudes the unpolarized differential cross section for the photodisintegration process is given by

$$\begin{aligned}
 \frac{d\sigma}{d\Omega}(q, \theta) &= m_N \hbar \frac{q E_{\gamma}}{3 \pi c} (2\pi)^3 \frac{1}{4} \\
 & \quad \times \sum_{M_S M_J} \sum_{\lambda M_{\Gamma}'} |\langle_S^{(-)} \langle \mathbf{q} S M_S; \psi_d j m_j | H_{\text{em}} | \\
 & \quad \times \Psi_{\text{BS}} \Gamma' M_{\Gamma'} \rangle_S|^2. \quad (21)
 \end{aligned}$$

The differential cross section is usually expanded in terms of Legendre polynomials

$$\sigma(q, \theta) = \frac{d\sigma}{d\Omega}(q, \theta) = A_0 \left(1 + \sum_{k=1}^4 a_k P_k(\cos \theta) \right). \quad (22)$$

The coefficients A_0 and a_k can be calculated analytically from Eqs. (20) and (21). The total cross section is obtained by integrating Eq. (22) over the angle θ between the incoming photon and the outgoing proton or neutron $\sigma = 4\pi A_0$.

The cross section for the p - d or n - d capture process is obtained from the corresponding photodisintegration expression by using the principle of detailed balance [33]

$$\frac{d\sigma^{\text{dis}}}{d\Omega} = \frac{3}{2} \frac{k^2}{Q^2} \frac{d\sigma^{\text{cap}}}{d\Omega}. \quad (23)$$

Here, k and Q are the momenta of the proton and the photon, respectively. In the present treatment no Coulomb forces have been taken into account, in other words the matrix elements of Eq. (1) for p - d capture differ from the corresponding n - d expression only in their isospin content.

III. RESULTS

It should be pointed out that we have shifted all theoretical cross sections to the experimental threshold for a meaningful comparison. All calculations are done with the theoretical binding energies.

In Fig. 1 we show our theoretical results for the total cross section of ${}^3\text{He}$ photodisintegration compared to most of the available experimental data [2–4,8–13] up to $E_{\gamma}=40$ MeV. Not shown are the data by van der Woude *et al.* [15] and Chang *et al.* [17] who found evidence for an excited state in their measurements. This resonance behavior has never been confirmed by any other group. It can be seen from Fig. 1 that there are large discrepancies between the different data sets around $E_{\gamma}=11$ MeV. The theoretical curves lie in between the data sets. It should be emphasized that for the calculated

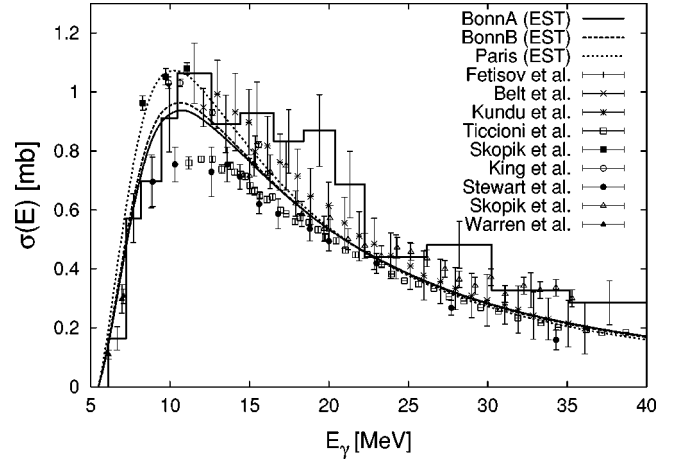


FIG. 1. Total cross section for the photodisintegration of ${}^3\text{He}$. The data are from Refs. [2–4,8–10,12–14,20].

curves there is a correlation between the three-body binding energy and the peak height of the cross section for the photodisintegration [42,43], i.e., the higher the binding energy the lower the cross section at the peak. Above 12 MeV the mentioned discrepancy of the experimental data declines. Due to the large error bars it is not possible to draw further conclusions.

In Fig. 2 we present total cross section calculations of photodisintegration of ${}^3\text{He}$ between $E_{\gamma}=40$ MeV and $E_{\gamma}=100$ MeV compared to the measurements of Fetisov *et al.* [4], Kundu *et al.* [9], Ticcioni *et al.* [10], and O’Fallon *et al.* [16]. For energies above $E_{\gamma}=60$ MeV the measured points lie slightly above our curves, computed by employing Bonn A, Bonn B, and Paris potentials. However, our curves agree with the tendency of the data.

We would like to point out that especially in this energy range a high rank representation of the NN potentials is required in order to get converged results. Below $E_{\gamma}=40$ MeV the improvements with respect to a low rank calculation are of the order of 1–5%. In view of the experimental error bars this change is of course not relevant. Above $E_{\gamma}=40$ MeV

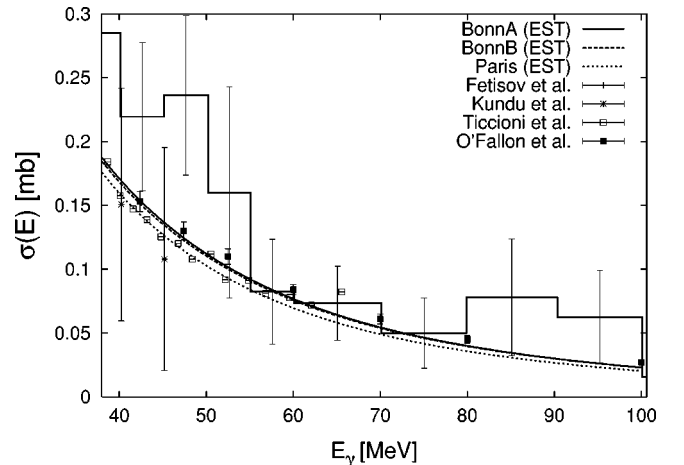


FIG. 2. Total cross section for the photodisintegration of ${}^3\text{He}$. The data are from Refs. [4,9,10,16].

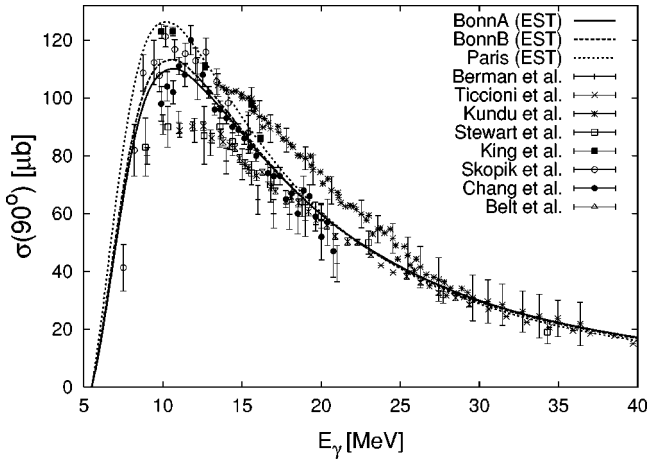


FIG. 3. Differential cross section at 90° for the photodisintegration of ^3He . The data are from Refs. [2,5,8–13].

the low rank calculations yield a cross section which is 5–15 % lower than the high rank calculations presented in this paper.

The differential cross section calculations at 90° for the photodisintegration of ^3He up to an energy of $E_\gamma=40$ MeV are illustrated in Fig. 3 in comparison to the corresponding experimental data [2,5,8–13]. The EST representations of the potentials Bonn A, Bonn B, and Paris are employed. As in the previous figures, we cannot observe any significant difference for energies above $E_\gamma=20$ MeV, whereas the peak region shows a considerable potential dependence, as discussed for Fig. 1. The data by Berman *et al.* [5] are below the calculated curves, however, they do agree with the tendency in the peak region. There is a remarkable discrepancy between these data sets and the data points measured by Kundu *et al.* [9], but they coincide with the theoretical curves for energies above 25 MeV. We find again that the theoretical results lie in between the data, though there are discrepancies between the data sets and, moreover, the error bars are quite large.

The two-body photodisintegration of ^3H has been mea-

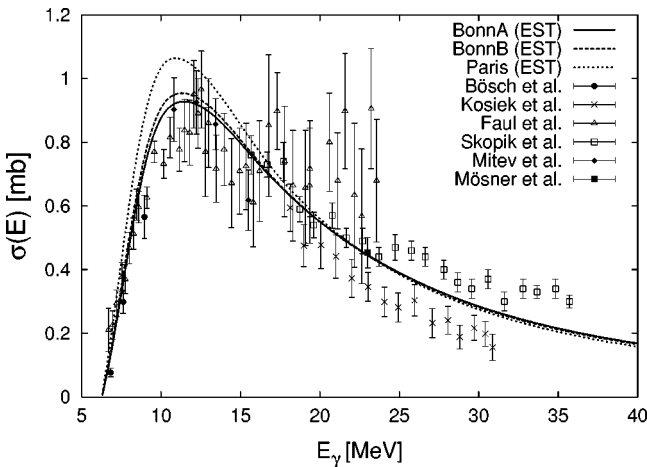


FIG. 4. Total cross section for the photodisintegration of ^3H . The data are from Refs. [22–28].

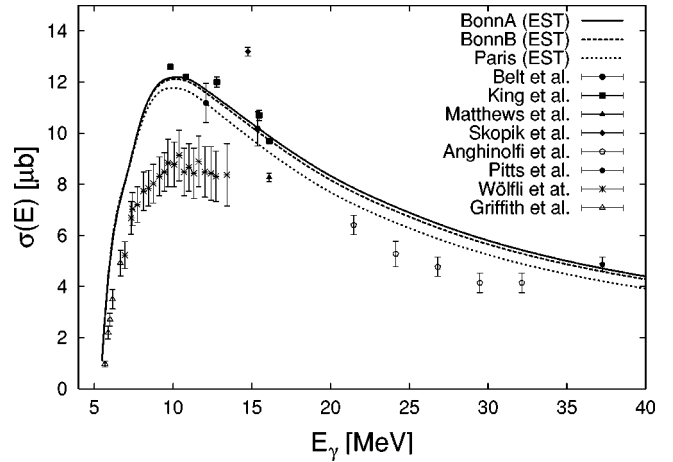


FIG. 5. Total cross section for the capture of protons by deuterons. The data are from Refs. [1,6–8,12,13,18,19,21].

sured by Bösch *et al.* [22], Kosiek *et al.* [23,24], Faul *et al.* [25], and Skopik *et al.* [26]. In Fig. 4 we display these data compared to our theoretical calculations. Also shown in this figure are the transformed results by Mitev *et al.* [27] and Mösner *et al.* [28] obtained from radiative n - d capture mea-

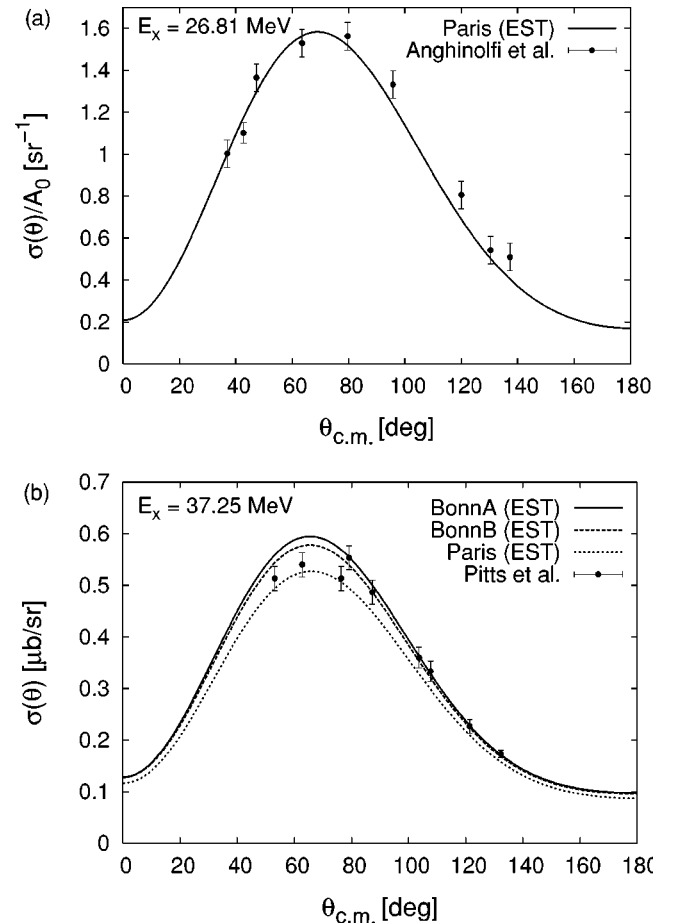


FIG. 6. Angular distribution and differential cross section for the capture of protons by deuterons. The data are from Refs. [19,21].

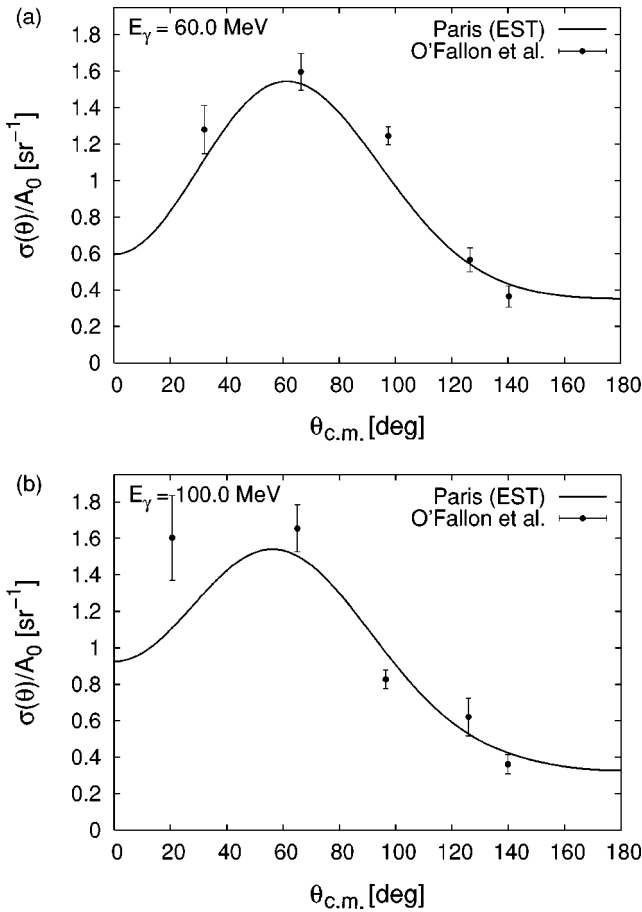


FIG. 7. Angular distribution and differential cross section for the photodisintegration ${}^3\text{He}$. The data are from Ref. [16].

measurements. It should be pointed out that the most recent measurement by Mösner *et al.* is in excellent agreement with the theory. We notice that for low energies, e.g., up to $E_\gamma = 15$ MeV, the calculated curves for the different potentials show a different behavior, whereas for higher energies all three calculations do not yield any significant difference. In the

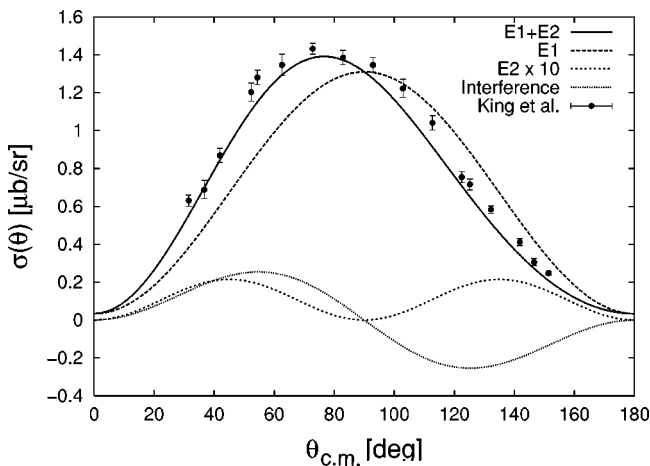


FIG. 8. Differential cross section for the capture of protons by deuterons at $E_p^{\text{lab}} = 10.93$ MeV for the Bonn B potential. The data are from Ref. [13].

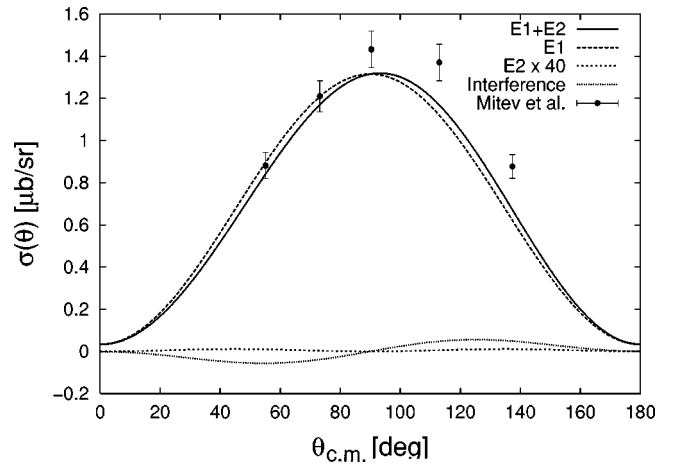


FIG. 9. Differential cross section for the capture of neutrons by deuterons at $E_n^{\text{lab}} = 10.8$ MeV for the Bonn B potential. The data are from Ref. [27].

peak region, the curves for the Bonn A and the Bonn B potentials cover the experimental data in between the error bars better. For energies above 20 MeV there is a large discrepancy between the data sets by Kosiek *et al.* and Skopik *et al.*, although the tendency of the data is similar. This indicates a normalization problem.

In Ref. [44] we discussed the available data for p - d capture below $E_x = 20$ MeV. It was shown that only the coefficient A_0 of the expansion in Eq. (22) has some potential dependence, whereas the coefficients a_k are almost independent from the interaction. Also in this case there is a correlation between the peak height and the binding energy, i.e., the lower the binding energy the lower the peak height. It should be pointed out that this is the inverse of the relation found in case of the photodisintegration. We also have demonstrated that there seems to be a normalization problem in the experimental data. It can be seen in Fig. 5 that the data by Wölfli *et al.* [6,7], Matthews *et al.* [18], and Anghinolfi *et al.* [19] are too low compared to those by King *et al.* [13], Pitts *et al.* [21], and Belt *et al.* [8] which agree with our theoretical curves. This indicates a calibration problem of the measurements. It was also shown in Ref. [44] that after renor-

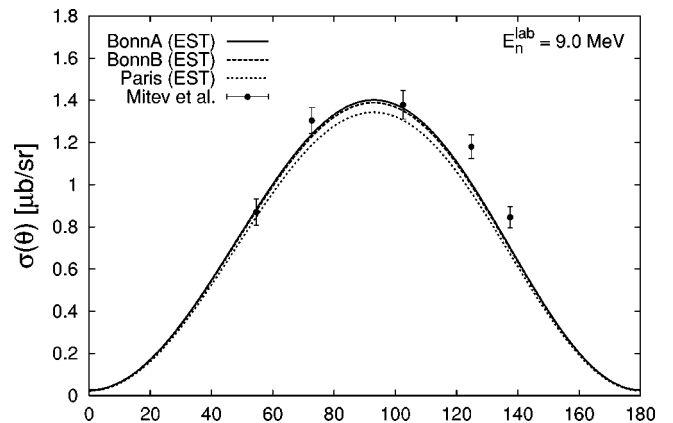


FIG. 10. Differential cross section for the capture of neutrons by deuterons. The data are from Ref. [27].

TABLE III. Coefficients for the expansion of the differential cross section for n - d capture for the Paris (EST) potential.

E_x [MeV]	A_0 [μb]	a_1	a_2	a_3	a_4
21.47	0.579	-0.071	-0.88	0.069	-0.0021
24.14	0.517	-0.065	-0.84	0.064	-0.0023
26.81	0.464	-0.057	-0.81	0.056	-0.0026
29.47	0.421	-0.047	-0.78	0.047	-0.0028
32.14	0.383	-0.035	-0.75	0.037	-0.0030

malization the data sets by Matthews *et al.* are in agreement with those by King *et al.* and the theoretical curves. At energies above $E_\gamma = 20$ MeV we encounter a similar problem and compare in Fig. 6 the differential cross section divided by A_0 . It can be seen that the agreement between theory and the experimental data by Anghinolfi *et al.* is very good. A comparison of the expansion coefficients obtained by Anghinolfi *et al.* and our theoretical values for the Paris (EST) potential is given in Table IV. There are discrepancies for A_0 which are connected to the normalization problem mentioned earlier. Despite the relatively big experimental error bars for the expansion coefficients a_k there are considerable good agreements.

Also shown in Fig. 6 are the data by Pitts *et al.* [21]. In this case there is also excellent agreement for the absolute cross section, particularly by employing the Bonn A potential. There are two additional data sets by van der Woude *et al.* [15] at $E_x = 19.2$ MeV and $E_x = 20.6$ MeV which are not shown here because of the measured resonance behavior, as mentioned above.

In addition to total cross section data, O'Fallon *et al.* [16] have also measured data sets of the differential cross section for photodisintegration of ${}^3\text{He}$ up to an energy of $E_\gamma = 140$ MeV. As can be seen in Fig. 2 their total cross sections are slightly higher than the theoretical predictions. For a meaningful comparison with our calculations we illustrate in Fig. 7 two of their data sets for the differential cross section normalized with A_0 . Within their error bars they agree quite well with the theoretical calculations.

The different contributions for the $E1$ and $E2$ transitions

in case of p - d capture at $E_p^{\text{lab}} = 10.93$ MeV are shown in Fig. 8. The pure $E2$ contributions are very small and enter the differential cross section essentially through the $E1$ - $E2$ interference term, which leads to the asymmetry, i.e., the curve is shifted to smaller angles. With the inclusion of $E2$ transitions there is an excellent agreement with the data by King *et al.* [13]. The only measurement of the angular distribution of the differential cross section for n - d capture has been done by Mitev *et al.* [27]. The different contributions for the $E1$ and $E2$ terms are shown in Fig. 9 for $E_n^{\text{lab}} = 10.8$ MeV. Due to isospin selection rules the $E2$ contribution, and hence the interference between the $E1$ and the $E2$ term, is much smaller compared to ${}^3\text{He}$. It should be noted that in this case the maximum of the differential cross section is shifted to larger angles. This observation was also made in Ref. [29] for the Born approximation. A comparison to the theoretical calculations at $E_n^{\text{lab}} = 9$ MeV is shown in Fig. 10. It can be seen from Figs. 9 and 10 that the peaks of the experimental data tend to have a bigger asymmetry than the theoretical curves. It is remarkable that this circumstance is independent of the potential choice. This indicates either a stronger contribution of a higher multipole, not present in our theoretical calculations, or an error in the data. To the best of our knowledge there are no other differential cross section data for ${}^3\text{H}$ photodisintegration or the inverse reaction available. There are also no experimental data available for the Legendre coefficients a_k . Nevertheless, we show for comparison in Table III corresponding calculated values for n - d capture at the same energies as the available data for p - d capture from Table IV. It can be seen that for n - d capture the angular distribution is dominated by the a_2 coefficient, i.e., the $E1$ transitions, whereas in case of p - d capture there are bigger admixtures of $E2$ contributions.

One observable of particular interest in the context of angular distributions is the so-called fore-aft asymmetry. This quantity is defined by

$$a_s = \frac{\sigma(54.7^\circ) - \sigma(125.3^\circ)}{\sigma(54.7^\circ) + \sigma(125.3^\circ)}. \quad (24)$$

TABLE IV. Coefficients for the expansion of the differential cross section for p - d capture. For each energy the first row corresponds to the theoretical results obtained with the Paris (EST) potential, and the second row contains the data from Ref. [19].

E_x [MeV]	A_0 [μb]	a_1	a_2	a_3	a_4
21.47	0.575	0.42	-0.83	-0.41	-0.05
	0.51 ± 0.03	0.28 ± 0.1	-0.82 ± 0.13	-0.38 ± 0.15	-0.07 ± 0.1
24.14	0.517	0.44	-0.79	-0.43	-0.05
	0.42 ± 0.04	0.34 ± 0.1	-0.86 ± 0.12	-0.35 ± 0.15	-0.12 ± 0.1
26.81	0.467	0.46	-0.75	-0.44	-0.06
	0.38 ± 0.03	0.41 ± 0.1	-0.86 ± 0.13	-0.39 ± 0.15	-0.11 ± 0.1
29.47	0.425	0.47	-0.72	-0.45	-0.06
	0.33 ± 0.03	0.39 ± 0.1	-0.77 ± 0.10	-0.42 ± 0.15	-0.12 ± 0.1
32.14	0.389	0.48	-0.68	-0.45	-0.07
	0.33 ± 0.03	0.33 ± 0.1	-0.79 ± 0.12	-0.36 ± 0.15	-0.08 ± 0.1

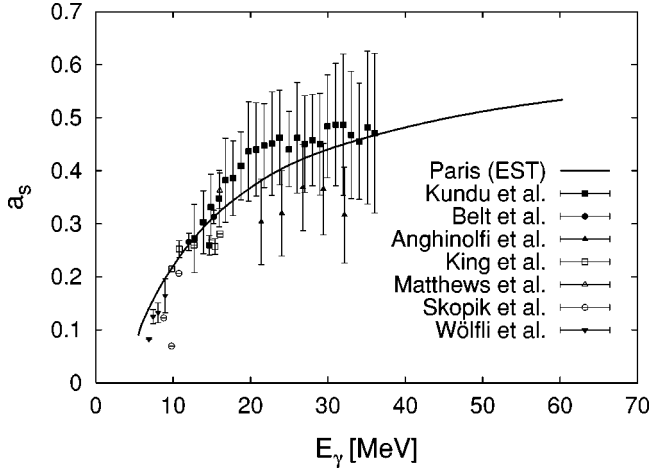


FIG. 11. Fore-aft asymmetry a_s for ${}^3\text{He}$ as defined in the text. The data are from Refs. [6–9,12,13,18–20].

In terms of Legendre polynomial expansion coefficients of Eq. (22), this can be written as

$$a_s = \frac{a_1 - \frac{2}{3}a_3}{\sqrt{3}\left(1 - \frac{7}{18}a_4\right)}. \quad (25)$$

In Figs. 11 and 12 we compare our results with the available data sets. The theoretical curves for ${}^3\text{He}$ agree quite well with the data [6–9,12,13,18–20], whereas the calculated asymmetry for ${}^3\text{H}$ is smaller by a factor of 5 than the experimental data [22,26,27]. A similar observation was made by Skopik *et al.* [20] using their effective capture calculations, where no FSI effects were taken into account. Since all experimental data show a consistently higher fore-aft asymmetry, there seems to be something missing in the theoretical description of this reaction. One possible explanation for the discrepancy between theory and experiment was that the FSI has not been taken into account properly in previous calculations. In the present calculations we have shown that this discrepancy still remains when taking FSI effects into account. Therefore, it is still unclear where the differences stem from. The $M1$ term is not likely to solve the problem, since it is only expected to have an effect at extreme angles or at very low energies. Also three-nucleon forces are not expected to solve the problem since the angular distribution shows no potential dependence. A possible solution could be the inclusion of explicit meson exchange currents which allow a stronger coupling of higher multipoles to ${}^3\text{H}$.

IV. CONCLUSIONS

In this paper we have analyzed all available experimental data for the photodisintegration of ${}^3\text{He}$ and ${}^3\text{H}$ and the cor-

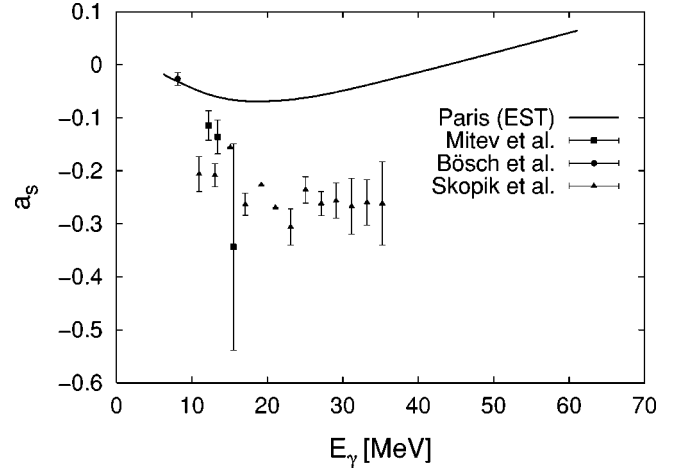


FIG. 12. Same as Fig. 11 but for ${}^3\text{H}$. The data are from Refs. [22,26,27].

responding inverse reactions below $E_\gamma = 100$ MeV by comparing with our calculations using realistic NN interactions. We have shown that the theoretical curves agree with the experimental data for the total cross section within the error bars. Moreover, in many cases the measured differential cross sections for p - d capture (aside from a normalization factor) can be explained theoretically over a large energy range. In Ref. [44] it was already shown that a similar normalization problem exists for the data below $E_x = 20$ MeV. There, it was also shown that the angular distribution is insensitive to the underlying two-body interaction, whereas there is a strong correlation between the three-body binding energy and the normalization constant A_0 [42,43]. Since the angular distribution is insensitive to the employed interaction, we do not expect large effects of three-nucleon forces. On the other hand taking account of them will change the three-body binding energy and hence the normalization constant A_0 .

For n - d capture the description of the angular distribution is less good. For energies above 10 MeV the theoretical results give a much smaller asymmetry than the experimental data. Hence, the theoretical fore-aft asymmetry shows a large discrepancy from the experimental data, whereas for p - d we achieve a very good agreement.

ACKNOWLEDGMENTS

The work of W.Sch. was supported by the Natural Science and Engineering Research Council of Canada. The work of O.N. was supported by the Graduiertenkolleg “Die Erforschung subnuklearer Strukturen der Materie.” W.Sch. acknowledges support and hospitality from the University of Padova during the write up of this paper. We thank L. Canton for providing computing time, which made the high rank calculations of this work possible.

- [1] G. M. Griffith, E. A. Larson, and L. P. Robertson, *Can. J. Phys.* **40**, 402 (1962).
- [2] J. R. Stewart, R. C. Morrison, and J. S. O'Connell, *Phys. Rev.* **138**, B372 (1963).
- [3] J. R. Warren, K. L. Erdman, L. P. Robertson, D. A. Axen, and J. R. Macdonald, *Phys. Rev.* **132**, 1691 (1963).
- [4] V. N. Fetisov, A. N. Gorbunov, and A. T. Varfolomeev, *Nucl. Phys.* **71**, 305 (1965).
- [5] B. L. Berman, L. J. Koester, and J. H. Smith, *Phys. Rev.* **133**, B117 (1964).
- [6] W. Wölfli, R. B. Bösch, J. Lang, and R. Müller, *Phys. Lett.* **22**, 75 (1966).
- [7] W. Wölfli, R. B. Bösch, J. Lang, R. Müller, and P. Marmier, *Helv. Phys. Acta* **40**, 946 (1967).
- [8] B. D. Belt, C. R. Bingham, M. L. Halbert, and A. van der Woude, *Phys. Rev. Lett.* **24**, 1120 (1970).
- [9] S. K. Kundu, Y. M. Shin, and G. D. Wait, *Nucl. Phys.* **A171**, 384 (1971).
- [10] G. Ticcioni, S. N. Gardiner, J. L. Matthews, and R. O. Owens, *Phys. Lett.* **46B**, 368 (1973).
- [11] C. C. Chang, W. R. Dodge, and J. J. Murphy II, *Phys. Rev. C* **9**, 1300 (1974).
- [12] D. M. Skopik, H. R. Weller, N. R. Roberson, and S. A. Wender, *Phys. Rev. C* **19**, 601 (1979).
- [13] S. King, N. R. Roberson, H. R. Weller, and D. R. Tilley, *Phys. Rev. C* **30**, 21 (1984).
- [14] S. King, N. R. Roberson, H. R. Weller, D. R. Tilley, H. P. Engelbert, H. Berg, E. Huttel, and G. Clausnitzer, *Phys. Rev. C* **30**, 1335 (1984).
- [15] A. van der Woude, M. L. Halbert, and C. R. Bingham, *Phys. Rev. Lett.* **26**, 909 (1971).
- [16] N. M. O'Fallon, L. J. Koester, Jr., and J. H. Smith, *Phys. Rev. C* **5**, 1926 (1972).
- [17] C. C. Chang, E. M. Diener, and E. Ventura, *Phys. Rev. Lett.* **29**, 307 (1972).
- [18] J. L. Matthews, T. Kruse, M. E. Williams, R. O. Owens, and W. Sawin, *Nucl. Phys.* **A223**, 221 (1974).
- [19] M. Anghinolfi, P. Corvisiero, M. Guarone, G. Ricci, and A. Zucchiatti, *Nucl. Phys.* **A410**, 173 (1983).
- [20] D. M. Skopik, J. Asai, D. H. Beck, T. P. Dielschneider, R. E. Pywell, and G. A. Retzlaff, *Phys. Rev. C* **28**, 52 (1983).
- [21] W. K. Pitts, H. O. Meyer, L. C. Bland, J. D. Brown, R. C. Byrd, M. Hugi, H. J. Karwowski, P. Schwandt, A. Sinha, J. Sowinski, I. J. van Heerden, A. Arriaga, and F. D. Santos, *Phys. Rev. C* **37**, 1 (1988).
- [22] R. B. Bösch, J. Lang, R. Müller, and W. Wölfli, *Phys. Lett.* **8**, 120 (1964); *Helv. Phys. Acta* **38**, 753 (1965).
- [23] R. Kosiek, D. Müller, and R. Pfeiffer, *Phys. Lett.* **21**, 199 (1966).
- [24] R. Pfeiffer, *Z. Phys.* **208**, 129 (1968).
- [25] D. D. Faul, B. L. Berman, P. Meyer, and D. L. Olson, *Phys. Rev. Lett.* **44**, 129 (1980).
- [26] D. M. Skopik, D. H. Beck, J. Asai, and J. J. Murphy II, *Phys. Rev. C* **24**, 1791 (1981).
- [27] G. Mitev, P. Colby, N. R. Roberson, and H. R. Weller, *Phys. Rev. C* **34**, 389 (1986).
- [28] J. Mösner, K. Möller, W. Pilz, G. Schmidt, and T. Stiehler, *Few-Body Syst.* **1**, 83 (1986).
- [29] D. J. Klepacki, Y. E. Kim, and R. A. Brandenburg, *Nucl. Phys.* **A550**, 53 (1988).
- [30] B. F. Gibson and D. R. Lehman, *Phys. Rev. C* **11**, 29 (1975).
- [31] E. O. Alt, P. Grassberger, and W. Sandhas, *Nucl. Phys.* **B2**, 167 (1967).
- [32] S. Aufleger and D. Drechsel, *Nucl. Phys.* **A364**, 81 (1983).
- [33] B. A. Craver, Y. E. Kim, and A. Tubis, *Nucl. Phys.* **A276**, 237 (1977).
- [34] J. L. Friar, B. F. Gibson, and G. L. Payne, *Phys. Lett. B* **251**, 11 (1990).
- [35] M. Viviani, R. Schiavilla, and A. Kievsky, *Phys. Rev. C* **54**, 534 (1996).
- [36] V. Efros, W. Leidemann, G. Orlandini, and E. L. Tomusiak, *Phys. Lett. B* **484**, 223 (2000).
- [37] J. Jourdan, M. Baumgartner, S. Burzynski, P. Egelhof, R. Henneck, A. Klein, M. A. Pickar, G. R. Plattner, W. D. Ramsay, H. W. Roser, I. Sick, and J. Torre, *Nucl. Phys.* **A453**, 220 (1986).
- [38] S. Ishikawa and T. Sasakawa, *Phys. Rev. C* **45**, R1428 (1992).
- [39] A. C. Fonseca and D. R. Lehman, in *Proceedings of the 14th International IUPAP Conference on Few-Body Problems in Physics*, Williamsburg, VA, 1994, edited by Franz Gross, AIP Conf. Proc. No. 334 (AIP, Woodbury, NY, 1995).
- [40] H. Anklin, L. J. de Bever, S. Buttazzoni, W. Glöckle, J. Golak, A. Honegger, J. Jourdan, H. Kamada, G. Kubon, T. Petitjean, L. M. Qin, I. Sick, P. Steiner, H. Witała, M. Zeier, J. Zhao, and B. Zihlmann, *Nucl. Phys.* **A636**, 189 (1998).
- [41] J. Golak, H. Kamada, H. Witała, W. Glöckle, J. Kuroś, R. Skibiński, V. V. Kotlyar, K. Sagara, and H. Akiyoshi, *nucl-th/0006048*.
- [42] W. Schadow and W. Sandhas, *Nucl. Phys.* **A631**, 588c (1998).
- [43] W. Sandhas, W. Schadow, G. Ellerkmann, L. L. Howell, and S. A. Sofianos, *Nucl. Phys.* **A631**, 210c (1998).
- [44] W. Schadow and W. Sandhas, *Phys. Rev. C* **59**, 607 (1999).
- [45] J. Haidenbauer and W. Plessas, *Phys. Rev. C* **30**, 1822 (1984).
- [46] J. Haidenbauer, Y. Koike, and W. Plessas, *Phys. Rev. C* **33**, 439 (1986).
- [47] W. Sandhas, in *Few-Body Systems, Supplement 1* (Springer-Verlag, Wien, 1986).
- [48] D. J. Ernst, C. M. Shakin, and R. M. Thaler, *Phys. Rev. C* **8**, 46 (1973); **9**, 1780 (1974).
- [49] Th. Januschke, T. N. Frank, W. Sandhas, and H. Haberzettl, *Phys. Rev. C* **47**, 1401 (1993).
- [50] W. Glöckle, *The Quantum Mechanical Few-Body Problem* (Springer-Verlag, Berlin, 1983).
- [51] C. de Boor, *A Practical Guide to Splines* (Springer, New York, 1978).
- [52] L. Canton and W. Schadow, *Phys. Rev. C* **56**, 1231 (1997).
- [53] W. Schadow, W. Sandhas, J. Haidenbauer, and A. Nogga, *Few-Body Syst.* **28**, 241 (2000).
- [54] A. J. F. Siegert, *Phys. Rev.* **52**, 787 (1937).
- [55] M. M. Giannini and G. Ricco, *Photoreactions above the Giant Dipole Resonances* (Springer, New York, 1985).
- [56] W. Schadow, Ph. D. thesis, Bonn University, Germany, Report No. BONN-IR-97-17, 1997.